Rotor Position Phase-Locked Loop for Decoupled P-Q Control of DFIG for Wind Power Generation

Bakari Mwinyiwiwa, *Member, IEEE*, Yongzheng Zhang, *Student Member, IEEE*, Baike Shen, *Member, IEEE*, and Boon-Teck Ooi, *Life Fellow, IEEE*

***Abstract*—Implementation of decoupled P-Q control of doubly fed induction generators requires the positions of the rotors to be known. The rotor position phase-lock loop (PLL) is an invention that extracts rotor position and speed simultaneously by "sensorless" means. The rotor position PLL is parameter-insensitive because, apart from an approximate value of the magnetization reactance, knowledge of the other parameters is not required for it to function. Experimental results obtained under noisy conditions demonstrate that it is also insensitive to noise.**

***Index Terms*—Decoupled P-Q control, doubly fed induction generator (DFIG), phase-lock loop (PLL), position encoder, renewable energy, wind turbine generators (WTGs), wound rotor induction machine.**

I. Introduction

ONE workhorse of the wind turbine generators (WTGs) is the doubly fed induction generator (DFIG). DFIGs of 1.5 MW rating are used widely, with their size reaching 5 MW and higher. The major attraction of DFIGs is that decoupled active and reactive (P-Q) power can be controlled by back-to-back voltage-source converters (VSCs) connected from the slip rings of the rotor windings, so that the cost of power electronic hardware is reduced to a factor of about 0.3, which is the maximum positive slip and negative slip for wind power acquisition.

Decoupled P-Q control from the rotor side requires instantaneous knowledge of the rotor position $\theta_m = \omega_m t + \delta_m$. In motor drives, the preference is for "sensorless" means, and therefore, there have been active research in sensorless DFIGs [1]–[5] also. The methods used are based on solving for the rotor position from the equations of the DFIG using knowledge of the machine parameters, and the instantaneous measurements of voltages and currents of the stator and rotor. This paper is the fourth iteration of a method [6]–[8] based on simultaneous phase-lock tracking of both the rotor speed ω_m and position δ_m from voltage and current measurements. Apart from the magnetization reactance, the method does not require knowledge of the stator and rotor resistances, and the stator and rotor leakage inductances. In fact, the accuracy of the magnetization reactance is not critical, and experiments show that when it is assumed to be infinite, as in [8], the method is still good if the operating currents are large compared to the magnetization current. Robustness is implicit because there is no resistance to change with heating or inductance to change with magnetic saturation.

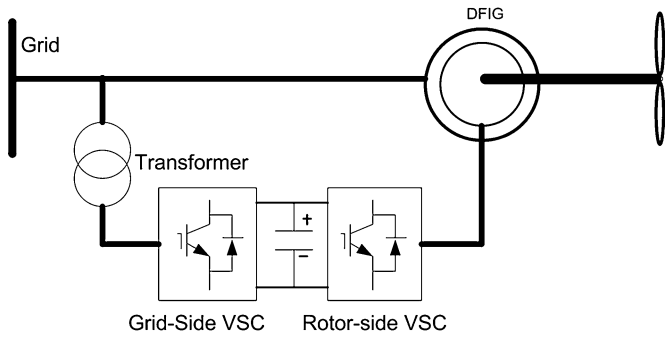

Fig. 1. DFIG with slip controls.

This paper is organized as follows. Section II gives an overview of decoupled P-Q control of DFIGs. Section III briefly reviews reference frame transformations, as it is an essential background to the understanding of the operation of the invention, which is described in Section IV. Section V returns to describe the integration of the invention to the decoupled P-Q controller. Section VI presents results of experimental tests on a DFIG based on a 5-hp wound rotor induction machine. The tests have been carried out in noisy conditions to prove its robustness.

II. Decoupled P-Q Control of DFIG

Fig. 1 is an illustration of a DFIG with the grid-side VSC and the rotor-side VSC. The grid-side VSC automatically conveys the slip power to the grid by using its active power control to maintain the regulated voltage across the dc capacitors. Little else needs to be added regarding the grid-side VSC because the control technique is well known.

The rotor-side VSC is assigned the task of decoupled P-Q control of the complex power $P_S + jQ_S$ of the stator-side of the induction generator. At this point, it needs to be stated that the "motor convention" is adopted so that negative P_S means generated active power. Neglecting ohmic losses, it is well known from induction motor theory that the real power crossing the air gap from the stator is $P_S = T_e \omega_{\rm syn}$, where T_e is the electromechanical torque and $\omega_{\rm syn}$ is the synchronous speed. The

Manuscript received October 12, 2007; revised November 10, 2008. Current version published August 21, 2009. This work was supported by the Natural Science and Engineering Research Council of Canada (NSERC) under Discovery Grant and Idea to Invention (I2I) Grant. Paper no. TEC-00370-2007.

B. Mwinyiwiwa is with the Department of Electrical Power Engineering, University of Dar Es Salaam, Dar es Salaam, Tanzania (e-mail: bakari@ee.udsm.ac.tz; bakari_mwinyiwiwa@yahoo.com).

Y. Zhang is with the Department of Electrical Engineering, McGill University, Montreal, QC H3A 2A7, Canada (e-mail: yongzheng.zhang@mail.mcgill.ca).

B. Shen is with the British Columbia Transmission Corporation, Vancouver, BC V7X 1V5, Canada (e-mail: baike.shen@bctc.com).

B.-T. Ooi is with the Department of Electrical and Computer Engineering, McGill University, Montreal, QC H3A 2A7, Canada (e-mail: boon-teck.ooi@mcgill.ca).

Digital Object Identifier 10.1109/TEC.2009.2025328

motoring power output is $P_m = T_e\omega_m$, where ω_m is the rotor speed. The remainder, $P_R = P_S - P_m$, is the real power from the rotor to the slip rings. Therefore, $P_R = (\omega_S - \omega_m)T_e = SP_S$, where the slip $S = (\omega_{\rm syn} - \omega_m)/\omega_{\rm syn}$.

For the *motor*, the rotor power is returned to the grid. Therefore, the power taken from the grid is $P_{\rm grid} = P_S - P_R = (1-S)P_S$. The active power taken by the stator from the grid is $P_S = P_{\rm grid}/(1-S)$. The formula derived for the *motoring* case applies for the *generating* case, with the direction of power transfer being taken care of by the change in polarity sign. The direction of active power through the rotor changes with slip.

Decoupled P-Q control is approached by using the γ–δ synchronously rotating frame equations given as shown (1) at the bottom of this page, where $L_s = L_{ls} + L_m$ and $L_R = L_{lR} + L_m$, and L_{ls} and L_{lR} being the leakage inductances.

The stator-side active power is $P_S = v_{S\gamma}i_{S\gamma} + v_{S\delta}i_{S\delta}$ and the reactive power is $Q_S = v_{S\gamma}i_{S\delta} - v_{S\delta}i_{S\gamma}$. Decoupled P-Q control is possible when $v_{S\delta} = 0$ in (1) can be assured. When $v_{S\delta} = 0$, $P_S = v_{S\gamma}i_{S\gamma}$ and $Q_S = v_{S\gamma}i_{S\delta}$. Under this decoupled condition, the stator complex power references P_S* and Q_S* can be controlled by the stator current references $i_{S\gamma}* = P_S*/v_{S\gamma}$ and $i_{S\delta}* = Q_S*/v_{S\gamma}$, respectively. The $*$ symbol denotes a control quantity. Since the DFIG is controlled from the rotor side, one looks for rotor control references. The rotor current references $i_{r\gamma}*$ and $i_{r\delta}*$ are obtained by solving the rotor currents from the first and second rows of (1). Neglecting the *d*/*dt* terms

$$\begin{pmatrix} i^*_{r\gamma} \\ i^*_{r\delta} \end{pmatrix} = \begin{pmatrix} (-\omega_s L_s i^*_{s\gamma} - R_s i^*_{s\delta})/\omega_s L_m \\ (-V_{S\gamma} - \omega_s L_s i^*_{s\delta} + R_s i^*_{s\gamma})/\omega_s L_m \end{pmatrix}. \quad (2)$$

Furthermore, assuming that the leakage inductances and the resistances are small compared to $\omega_S L_m$, (2) is approximated as

$$\begin{pmatrix} i^*_{r\gamma} \\ i^*_{r\delta} \end{pmatrix} \approx -\begin{pmatrix} i^*_{s\gamma} \\ i^*_{s\delta} \end{pmatrix} + \begin{pmatrix} 0 \\ -v_{S\gamma}/L_m\omega_S \end{pmatrix}. \quad (3)$$

The method used in this paper depends on ensuring that $v_{S\delta} = 0$ is satisfied. In this, it is necessary to track, $\theta_m = \omega_m t + \delta_m$, the angle between the axis of the stator a-phase and the rotor a-phase. This is because the α–β reference frame of rotor windings are carried around by the position of the rotor iron θ_m. The angle θ_m disappears after the transformation from the α–β frame to the d–q frame, and thereafter, transformation to the γ–δ frame. Therefore, in the reverse transformation from the γ–δ frame to the α–β frame, it is necessary to recover $\theta_m = \omega_m t + \delta_m$.

This paper extracts from the stator current measurements and the rotor current measurements, the instantaneous position of the stator flux vector, $\theta_S = \omega_S t + \delta_S$, with respect to the stator iron, and the instantaneous position of the rotor flux vector, $\theta_r = \omega_r t + \delta_r$, with respect to the rotor iron. Unlike other papers [1]–[5], the method used in this paper is based on the phase-lock loop (PLL) principle. Through the equivalent of the *voltage-controlled oscillator (VCO)* in the PLL, it introduces an algebraic unknown angle $\theta_X = \omega_X t + \delta_X$. At the equivalent of the *detector* of the PLL, it extracts the error $\varepsilon_X = \theta_S - (\theta_r + \theta_X)$. The error is applied to increase θ_X in negative feedback until $\theta_S - (\theta_r + \theta_X) = 0$. For the error to be zero, it is required that $\omega_S - (\omega_r + \omega_X) = 0$. From induction machine theory, $\omega_S - (\omega_r + \omega_m) = 0$. This means that $\omega_X = \omega_m$, i.e., the speed is measured without a tachometer. At this point, the axes of the stator and the rotor γ–δ frames are rotating at the same speed, but they are still not aligned. There is still an equation $\delta_S - (\delta_r + \delta_X) = 0$ to be satisfied, except that one needs a signpost to fasten the rotor γ–δ axes to. The reasoning used is: if $v_{S\delta} = 0$ yields the current conditions given by (3), then satisfying (3) implies that $v_{S\delta} = 0$. Therefore, (3) is used as the criterion of phase lock.

III. Reference Frame Transformations

After transformation from the a–b–c frame, the stator and rotor current vectors in the α–β frame are

$$\begin{bmatrix} i_{S\alpha} \\ i_{S\beta} \end{bmatrix} = \begin{bmatrix} I_S\cos(\omega_S t + \delta_{iS}) \\ I_S\sin(\omega_S t + \delta_{iS}) \end{bmatrix} \quad (4)$$

$$\begin{bmatrix} i_{r\alpha} \\ i_{r\beta} \end{bmatrix} = \begin{bmatrix} I_r\cos(\omega_r t + \delta_{ir}) \\ I_r\sin(\omega_r t + \delta_{ir}) \end{bmatrix}. \quad (5)$$

Fig. 2(a) is drawn to highlight $\theta_m = \omega_m t + \delta_m$, which is tracked by the method used in this paper.

By applying the transformation matrix $[e^{j\theta_m}]$

$$[e^{j\theta_m}] = \begin{bmatrix} \cos\theta_m & -\sin\theta_m \\ \sin\theta_m & \cos\theta_m \end{bmatrix} \quad (6)$$

where $\theta_m = \omega_m t + \delta_m$, the resultant d–q rotor current vector is

$$\begin{bmatrix} i_{rd} \\ i_{rq} \end{bmatrix} = \begin{bmatrix} I_r\cos(\omega_r t + \delta_{ir} + \omega_m t + \delta_m) \\ I_r\sin(\omega_r t + \delta_{ir} + \omega_m t + \delta_m) \end{bmatrix}. \quad (7)$$

As illustrated in Fig. 2(b), the angle $\theta_m = \omega_m t + \delta_m$ has disappeared in the d–q frame, so that it has to be recovered in the back-transformation. From induction machine theory, $\omega_S = \omega_m + \omega_r$, so that the magnetic flux produced by the stator currents $[\,i_{Sd},\quad i_{Sq}\,]^T$ and the rotor currents $[\,i_{rd},\quad i_{rq}\,]^T$ are both rotating at a synchronous speed ω_S.

In transforming to the γ–δ frame, the rotational transformation matrix

$$[e^{-j\theta_S}] = \begin{bmatrix} \cos\theta_S & \sin\theta_S \\ -\sin\theta_S & \cos\theta_S \end{bmatrix} \quad (8)$$

where $\theta_S = \omega_S t$ is multiplied to $[\,i_{Sd},\quad i_{Sq}\,]^T$ and $[\,i_{rd},\quad i_{rq}\,]^T$. Therefore, the resultant vectors in the γ–δ frame are $[\,i_{S\gamma},\quad i_{S\delta}\,]^T = [I_S\cos\delta_{iS}, I_S\sin\delta_{iS}]^T$ for the stator

$$\begin{pmatrix} v_{s\gamma} \\ v_{s\delta} \\ v_{r\gamma} \\ v_{r\delta} \end{pmatrix} = \begin{pmatrix} R_s + \frac{d}{dt}L_s & -\omega_s L_s & \frac{d}{dt}L_m & -\omega_s L_m \\ \omega_s L_s & R_s + \frac{d}{dt}L_s & \omega_s L_m & \frac{d}{dt}L_m \\ \frac{d}{dt}L_m & -(\omega_s - \omega_m)L_m & R_R + \frac{d}{dt}L_R & -(\omega_s - \omega_m)L_R \\ (\omega_s - \omega_m)L_m & \frac{d}{dt}L_m & (\omega_s - \omega_m)L_R & R_R + \frac{d}{dt}L_R \end{pmatrix} \begin{pmatrix} i_{s\gamma} \\ i_{s\delta} \\ i_{r\gamma} \\ i_{r\delta} \end{pmatrix} \quad (1)$$

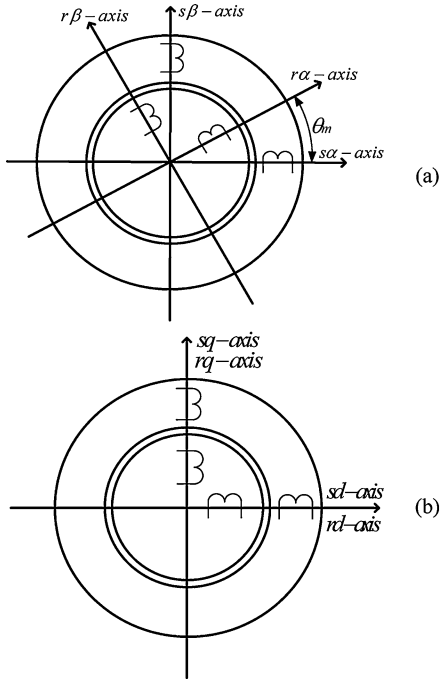

Fig. 2. Relationship of stator and rotor windings. (a) α–β frame. (b) d–q frame.

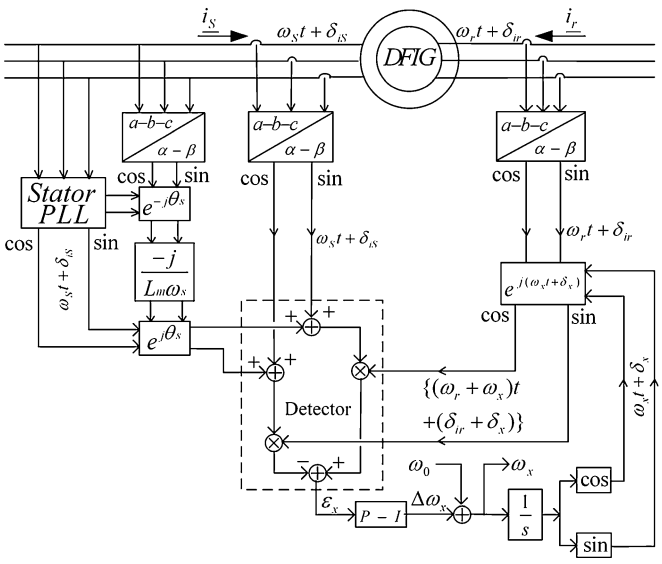

Fig. 3. Schematic of rotor position PLL.

currents and $[\, i_{r\gamma} \quad i_{r\delta}\,]^T = [I_r \cos(\delta_{ir} + \delta_m), I_r \sin(\delta_{ir} + \delta_m)]^T$ for the rotor currents.

IV. Rotor Position PLL

Fig. 3 is the schematic of the rotor position PLL. Its inputs are the three-phase stator currents, the three-phase rotor currents, the three-phase stator voltages, and the stator voltage PLL. Its outputs are the estimates of rotor speed and position $\theta_m = \omega_m t + \delta_m$. In three-phase PLLs, the a–b–c quantities are converted to two-phase α–β quantities.

A. Stator PLL

The output of a traditional three-phase PLL is originally an algebraic unknown angle $(\omega_y t + \delta_y)$. When the PLL tracks the three-phase stator voltage, the error between the angle $(\omega_{\rm SV} t + \delta_{\rm SV})$ of the stator voltage and $(\omega_y t + \delta_y)$ is detected. Then, the error changes ω_y and δ_y in negative feedback manner to null the error. Ultimately, $(\omega_y t + \delta_y)$ converges to $(\omega_{\rm SV} t + \delta_{\rm SV})$.

B. Rotor Position PLL

The same principle is applied to the rotor position PLL, except that the algebraic unknown $(\omega_X t + \delta_X)$ is added to the rotor current angle $(\omega_{ir} t + \delta_{ir})$, so that the angle $[(\omega_{ir} + \omega_X)t + \delta_{ir} + \delta_X)]$ is made to track the angle $(\omega_S t + \delta_S)$ of the stator currents. On convergence, $(\omega_X t + \delta_X)$ yields the angle of rotation of the rotor, which is $\theta_m = \omega_m t + \delta_m$.

Fig. 3 depicts two-phase information channels. The cos(·) and sin(·) symbols under the transformation blocks denote the channels containing the cosine and the sine of arguments, the arguments being the angles $\theta_x = \omega_x t + \delta_x$, $\theta_r = \omega_r t + \delta_r$, or $\theta_S = \omega_S t + \delta_S$, which are placed by the sides of the channel lines.

C. Criterion of Phase Lock

Because decoupled P-Q control assumes that $v_{S\delta} = 0$ and (3) is the consequence, the criterion of locking is based on (3). The resultant space vector $\boldsymbol{I_S}$ formed by the stator-side currents

$$\begin{pmatrix} i_{s\gamma} \\ i_{s\delta} \end{pmatrix} + \begin{pmatrix} 0 \\ v_{S\gamma}/L_m\omega_S \end{pmatrix}$$

is shown in Fig. 4(a). The resultant space vector $\boldsymbol{I_R}$ formed by the rotor-side currents

$$\begin{pmatrix} i_{r\gamma} \\ i_{r\delta} \end{pmatrix}$$

is shown in Fig. 4(b). As Fig. 4(a) and (b) illustrate, the γ–δ axes of the stator and the rotor are not, in general, aligned. By aligning the space vector $\boldsymbol{I_R}$ to the space vector $\boldsymbol{I_S}$, as illustrated in Fig. 4(c), both the γ–δ axes are coincident so that (1) is valid.

D. Magnetization Currents

The magnetization currents are not measured, and are obtained by making use of the γ–δ frame stator voltages obtained from measurements and dividing them by the magnetization reactance $jL_m\omega_S$. The stator voltages after a–b–c to α–β transformation become the vector $V_S[\cos(\omega_S t), 0]^T$. As shown in Fig. 3, the α–β frame stator voltages (which is the same as the d–q frame) are then transformed to the γ–δ frame stator voltages by using the $[e^{-j\theta_S}]$ block. The angle $\theta_S = \omega_S t$ of the $[e^{-j\theta_S}]$ block is obtained from the stator voltage PLL. The stator voltage PLL outputs the vector of reference angles $[\cos(\omega_S t),\ \sin(\omega_S t)]^T$. The resultant γ–δ frame stator voltage vector is $[\, v_{s\gamma} \quad 0\,]^T$. In order to obtain

$$\left(- \begin{pmatrix} 0 \\ \frac{v_{S\gamma}}{L_m\omega_S} \end{pmatrix} \right)$$

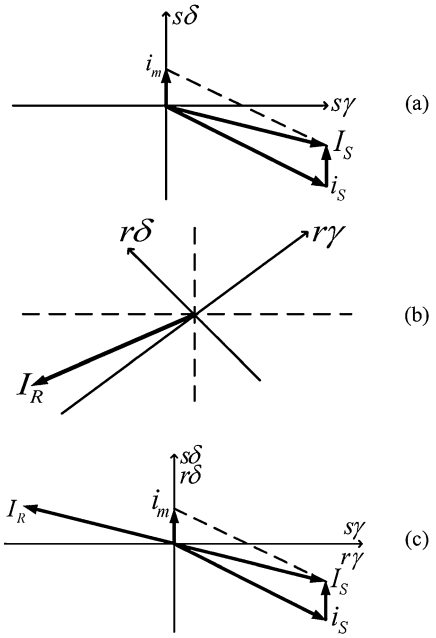

Fig. 4. Criterion of phase angle lock.

the stator voltage vector is multiplied by

$$\begin{bmatrix} 0 & 1 \\ \dfrac{-1}{L_m \omega_S} & 0 \end{bmatrix}.$$

The γ–δ frame magnetization current vector is transformed to the d–q frame by $[e^{j\theta_S}]$ to yield the d–q frame magnetization current vector

$$\begin{bmatrix} i_{md} \\ i_{mq} \end{bmatrix} = \begin{bmatrix} I_M \cos(\omega_S t + \delta_M) \\ I_M \sin(\omega_S t + \delta_M) \end{bmatrix}. \tag{9}$$

E. Stator Currents

After a–b–c to α–β transformation, the d–q frame stator current vector is

$$\begin{bmatrix} i_{Sd} \\ i_{Sq} \end{bmatrix} = \begin{bmatrix} I_S^1 \cos(\omega_S t + \delta_{iS}) \\ I_S^1 \sin(\omega_S t + \delta_{iS}) \end{bmatrix}. \tag{10}$$

F. Stator-Side Inputs to PLL

Combining (9) and (10), the stator-side inputs are

$$\begin{bmatrix} i_{Sd+m} \\ i_{Sq+m} \end{bmatrix} = \begin{bmatrix} I_S^1 \cos(\omega_S t + \delta_{iS}) \\ I_S^1 \sin(\omega_S t + \delta_{iS}) \end{bmatrix} + \begin{bmatrix} I_M \cos(\omega_S t + \delta_M) \\ I_M \sin(\omega_S t + \delta_M) \end{bmatrix} = \begin{bmatrix} I_S \cos(\omega_S t + \delta_S) \\ I_S \sin(\omega_S t + \delta_S) \end{bmatrix}. \tag{11}$$

G. Rotor Currents

After a–b–c to α–β transformation, the rotor current vector is

$$\begin{bmatrix} i_{r\alpha} \\ i_{r\beta} \end{bmatrix} = \begin{bmatrix} I_r \cos(\omega_r t + \delta_{ir}) \\ I_r \sin(\omega_r t + \delta_{ir}) \end{bmatrix}. \tag{12}$$

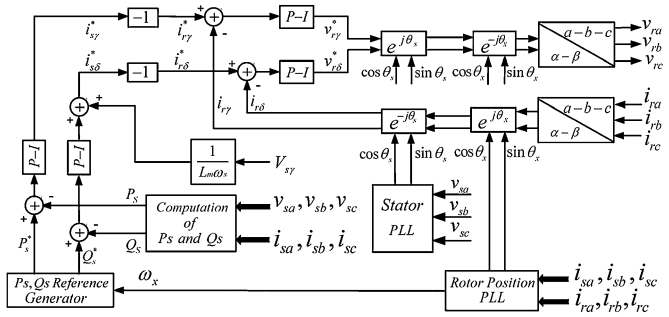

Fig. 5. Block diagram of rotor-side VSC control.

The stator currents are at frequency ω_S, whereas the rotor currents are at frequency ω_r. When the rotor currents are passed through the $[e^{j\theta_x}]$ block, where $\theta_x = \omega_x t + \delta_x$, the rotor currents become

$$\begin{bmatrix} i_{rd+x} \\ i_{rq+x} \end{bmatrix} = \begin{bmatrix} I_r \cos(\omega_r t + \delta_{ir} + \omega_x t + \delta_x) \\ I_r \sin(\omega_r t + \delta_{ir} + \omega_x t + \delta_x) \end{bmatrix}. \tag{13}$$

H. Detector of PLL

The inputs $[i_{Sd+m} \quad i_{Sq+m}]^T$ from (11) and $[i_{rd+x} \quad i_{rq+x}]^T$ from (13) meet at the detector of the PLL whose output is based on the operation

$$\varepsilon_x = i_{Sq+m} i_{rd+x} - i_{Sd+m} i_{rq+x}. \tag{14}$$

Substituting (11) and (13) in (14), it can be shown that $\varepsilon_x = I_S I_r \sin[(\omega_S - \omega_r - \omega_x)t + (\delta_S - \delta_r - \delta_x)]$. The error ε_x, after passing through the proportional–integral (P-I) block, yields the signal $\Delta\omega_X$. On adding a central frequency ω_0, the speed estimate $\omega_x = \omega_0 + \Delta\omega_x$ is formed. After passing through an integrator, one arrives at the position estimate $\theta_x = \omega_x t + \delta_x$, where δ_x is the constant of integration. The algebraic unknown θ_x is used as an address of cosine and sine lookup tables that outputs the vector $[\cos(\omega_x t + \delta_x), \sin(\omega_x t + \delta_x)]^T$.

The error ε_x causes $\Delta\omega_X$ and δ_x to change until $(\omega_S - \omega_r - \omega_x)t + (\delta_S - \delta_r - \delta_x) = 0$. When $\varepsilon_x = 0$, it means that $(\omega_S - \omega_r - \omega_x) = 0$ and $(\delta_S - \delta_r - \delta_x) = 0$. From induction machine theory and Section III, the following relationships always hold: $(\omega_S - \omega_r - \omega_m) = 0$ and $(\delta_S - \delta_r - \delta_m) = 0$. Therefore, $\omega_x = \omega_m$ and $\delta_x = \delta_m$. Thus, the rotor position PLL tracks the rotor position $\theta_x = \omega_m t + \delta_m$. The information $\theta_x = \omega_m t + \delta_m$ feeds the blocks $[e^{j\theta_x}]$ and $[e^{-j\theta_x}]$ in Fig. 5.

V. Rotor-Side Decoupled P-Q Control

Fig. 5 shows the rotor-side control that implements the decoupled P-Q control. Because the block diagram is similar to that in other publications, little needs to be added in explanation except to point out the phase angle of the $[e^{\pm j\theta_S}]$ transformation blocks comes from the stator voltage PLL and the phase angle of the $[e^{\pm j\theta_x}]$ transformation blocks comes from the rotor position PLL.

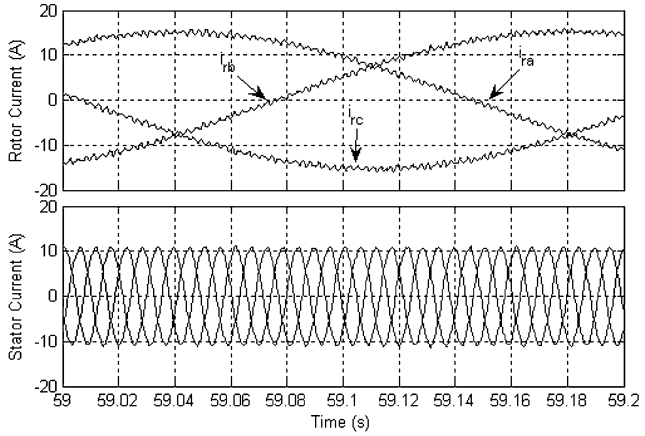

Fig. 6. Experimental three phase current waveforms. (a) Rotor (2.4 Hz). (b) Stator (60 Hz).

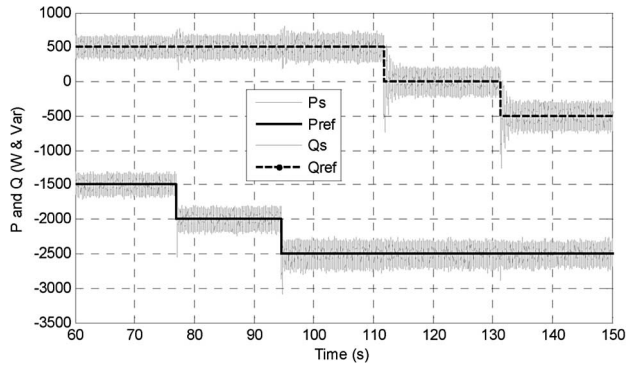

Fig. 7. Experimental results on responses to step changes in stator references $P_{\rm ref}$ and $Q_{\rm ref}$.

VI. Experimental Test Results

The prototype is tested in a noisy environment to show that the rotor position PLL is insensitive to noise as it tracks the rotor position in implementing the decoupled P-Q control.

Fig. 6 shows quality of rotor currents at slip frequency in (a) and the 60-Hz stator currents in (b).

A. Proof of P-Q Decoupling

Fig. 7 shows the stator complex power P_S and Q_S of the prototype in response to step changes in references $P_{\rm ref}$ and $Q_{\rm ref}$. Note that negative real power P_S denotes generated power. Also note that the time axis ranges from 60 to 150 s, so that the noise fluctuations that are not evident in Fig. 6 are present in Fig. 7. The experiment has been planned to demonstrate the decoupling of the P and the Q control over a wide operating range. In a step change of $P_{\rm ref}$, for instance, Q_S is only disturbed briefly. The converse applies.

As a control, an experiment has been performed with the slip rings of the wound rotor induction machine connected to a three-phase resistance bank. In this experiment, the wound rotor machine operates simply as a motor. The measurements of P_S and Q_S also show the noise fluctuations of Fig. 7. The noise in

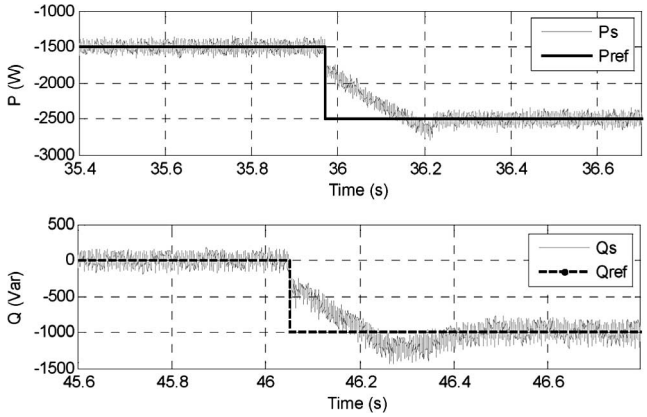

Fig. 8. Experimental results on complex power step response. (a) Real power. (b) Reactive power.

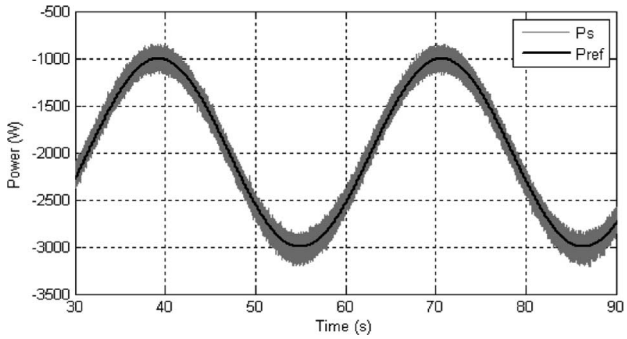

Fig. 9. Experimental results on tracking capability of P_S.

P_S and Q_S are due to noise from slight unbalance in the power supply, magnetic saturation, and mechanical vibrations.

B. Speed of Step Response

Fig. 8(a) shows, on an expanded time scale, the response of P_S due to a step change in the reference. The response of Q_S is not recorded. Fig. 8(b) shows the response of Q_S due to a step change of its reference in an entirely separate experiment. The settling time of P_S is within 0.26 s and that of Q_S is within 0.36 s. As the wind turbine blades have moments of inertia with time constants of $H = 4$ s, no effort has been made to shorten the response time.

C. Tracking Capability

In wind farm operation, P_S of the DFIG is expected to track a reference $P_{\rm ref}$ determined by a control strategy of the user. Fig. 9 demonstrates this capability in the generated power range from 1 to 3 KW, the latter being 80% of the rating of the induction machine. As the power to implement this experiment comes from the dc-chopper-driven dc motor, a higher power output and a higher oscillating frequency are not within the reach of our laboratory.

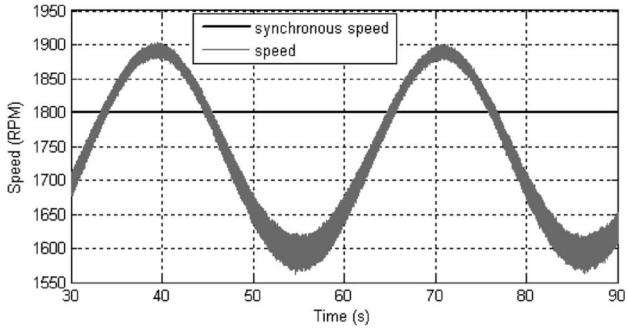

Fig. 10. Experimental measurements of rotor speed $\omega_x \approx \omega_m$.

D. Speed Measurement

In the same experiment in which Fig. 9 was recorded, the estimate of rotor speed $\omega_x \approx \omega_m$ was also recorded, and is shown in Fig. 10. The synchronous speed of 1800 r/m is shown in Fig. 10 to bring home the point that the power used in Fig. 9 is generated partly at subsynchronous speed and partly at supersynchronous speed. The noise in ω_x comes from the noise in the stator and rotor currents. Unlike the rotor position, the rotor speed is not essential in the implementation of decoupled P-Q control. In many control strategies, as shown in Fig. 5, rotor speed is used only as a pointer to the lookup tables in the $P_{\rm ref}(\omega_m)$ and $Q_{\rm ref}(\omega_m)$ references. A low-pass filter can remove the noise without affecting the control stability, as has been verified experimentally.

It is well known that PLLs are good filters of noise. The first stage of filtering is the P-I block after the detector in Fig. 3. But its output is a relatively noisy speed estimate $\Delta\omega_X$, which added to ω_0 yields ω_X. The second stage is the $1/S$ integrator block, so that δ_X has significant reduction. For instance, it reduces the fifth harmonic noise by $5 \times 60 \times 2\pi = 1884$.

E. Insensitiveness to Measurement Noise

Based on using the software position transducer as reference, Fig. 11 shows that the error of the *rotor position PLL* is around 0.11°, an accuracy lying between an 11- and a 12-bit absolute position encoder. The noise in the current measurement appears as fluctuation around the average, which is the estimated position by *rotor position PLL*. In order to show that the *rotor position PLL* is insensitive to noise, at $t = 14$ s, the three-phase ac voltage supply of the DFIG injects fifth and seventh voltage harmonics, each in the order of 10%. The average is not changed. Once the transient has subsided, the increased amount of noise appears as a slight increase in the fluctuation about the average.

F. Proof on Insensitivity to Parameter Variation

Fig. 12 displays experimental results in tests similar to Fig. 7, but with the difference that the magnetization inductance of 105.1 mH of the test machine (see Appendix B) has been replaced by $L_m\omega_S = \infty$. Fig. 12 is proof of the high insensitiveness to variation in the magnetization reactance. But instability sets in operation at low-power rating when the stator and rotor currents are small when compared to the magnetization current.

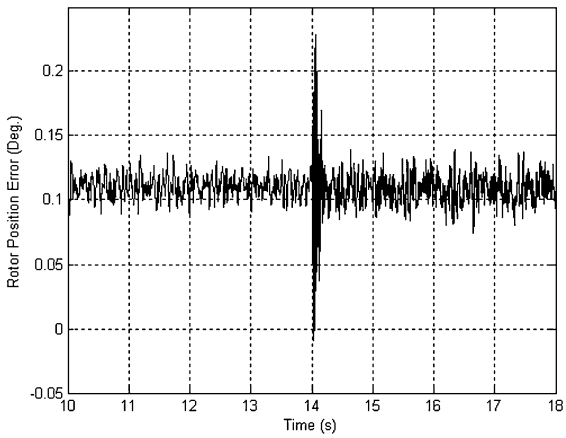

Fig. 11. Simulation of position error $\varepsilon_{\rm position}$.

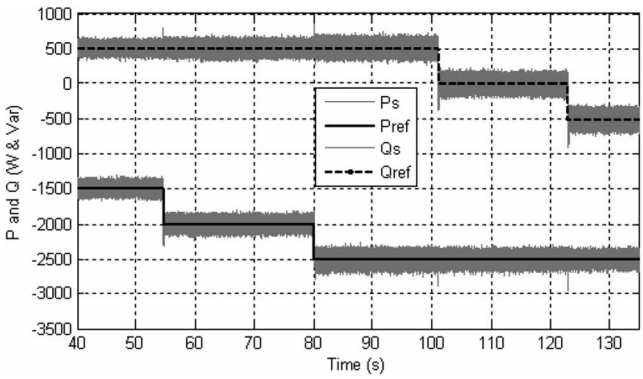

Fig. 12. Experimental results on the operation of the prototype in the model which assumes $L_m\omega_S = \infty$.

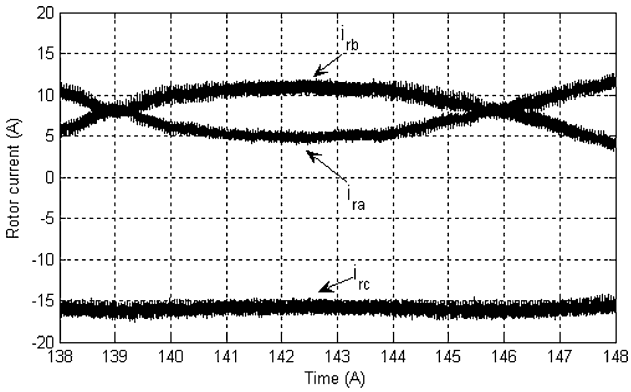

Fig. 13. Experimental rotor current waveforms at synchronous speed.

It should be remembered that no other machine parameter apart from the magnetization reactance is required.

G. Operation at Synchronous Speed

During conferences [6]–[8] in which the earlier iterations of the rotor position PLL were presented, doubts were raised as to its ability to track at synchronous speed. Fig. 13 shows the experimental measurement of the three-phase rotor currents for a 10-s-long duration when the speed is held synchronous. A slight and slow variation of the rotor voltage angle is evident

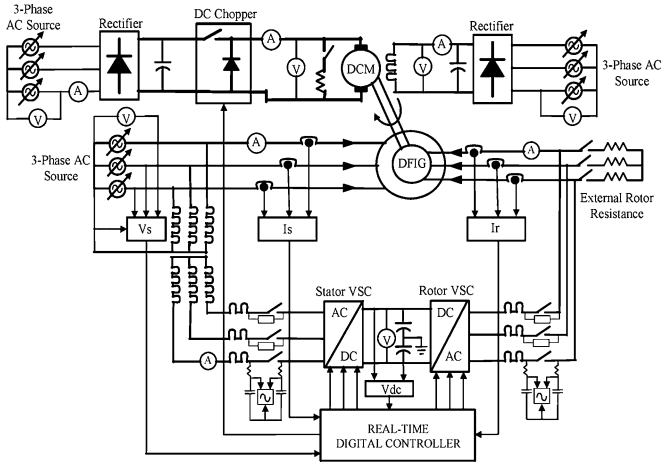

Fig. 14. Circuit layout of experimental test equipment.

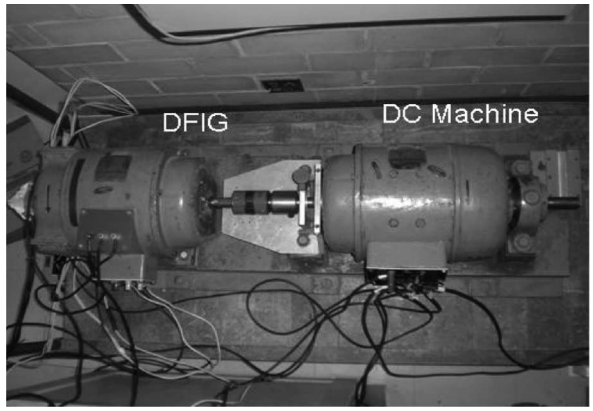

Fig. 15. Laboratory DFIG and dc machine.

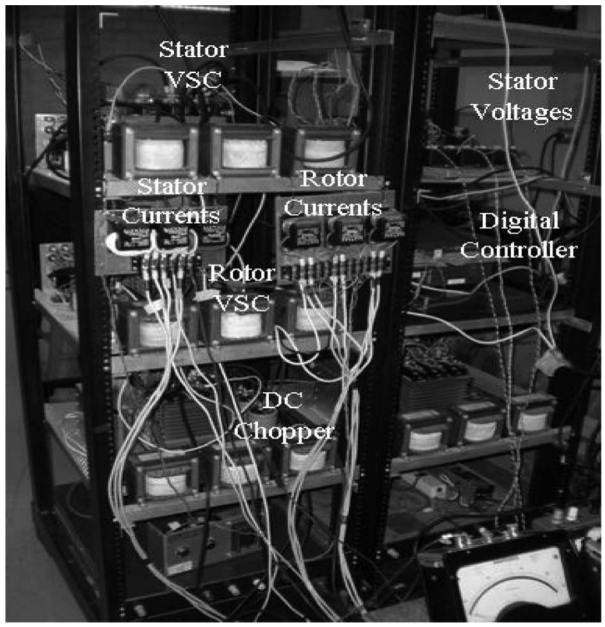

Fig. 16. Laboratory power electronics converters and digital controller.

in Fig. 13. The poor waveform appearance is because the 10-s duration is compressed within the display window.

VII. Conclusion

This paper has described the principle of operation of the rotor position PLL, which acquires the rotor position and rotor speed simultaneously, which is a vital information for the implementation of decoupled P-Q control in the DFIG. The rotor position PLL is designed to operate without the knowledge of any parameter of the DFIG except the magnetization reactance. A prototype has been assembled and tested. The experimental tests in a noisy environment are strong proofs that the invention is robust and insensitive to measurement noise.

Appendix A
Experimental Test Equipment

The experimental tests of the DFIG were conducted using a 5-hp wound rotor induction machine coupled to a 3.5-kW dc machine. The power electronics consists of three sets of VSCs. In the experiments, one VSC was connected to the stator side of the DFIG via a step-up transformer. The other VSC was connected to the rotor side of the DFIG. The third VSC was used as a chopper to control the armature voltage of the dc machine when used as a prime mover. Switching frequency of 1260 Hz and dc-link voltage of 185 V_{dc} have been used.

Fig. 14 shows the circuit layout of the laboratory experimental prototype. Fig. 15 shows the DFIG coupled to the dc machine. Fig. 16 shows the power electronics converters and the digital controller.

Appendix B
Parameters of DFIG and DC Machine

DFIG (Wound Rotor Induction Machine)

Measured parameters: $R_s = 0.431\,\Omega$, $R_r = 0.900\,\Omega$, $L_{ls} = L_{lr} = 2.12$ mH, and $L_m = 105.1$ mH.

DFIG name plate: 5 hp, 1700 r/m, 220 V, 13.5 A stator current, 60 Hz, 40 °C temperature rise. *Rotor:* 153 V, 15 A.

DC machine name plate: 3.5 kW, 1750 r/m, 220 V shunt winding (used as separately excited dc machine) 16 A armature current, 40 °C temperature rise, 0.75 A field current.

Acknowledgment

Dr. Bakari Mwinyiwiwa thanks the University of Dar-es-Salaam, Tanzania, for leave of absence to do research in McGill University. The authors would like to thank Prof. G. Joos for the use of real-time hardware-in-the-loop equipment and Mr. K. Gogas for initiating them on its use.

References

[1] L. Xu and W. Cheng, "Torque and reactive power control of a doubly fed induction machine by position sensorless scheme," *IEEE Trans. Ind. Appl.*, vol. 31, no. 3, pp. 636–642, May/Jun. 1995.

[2] R. Pena, J. C. Clare, and G. M. Asher, "Doubly fed induction generator using back-to-back PWM converters and its application to variable-speed wind-energy generation," *Proc. Inst. Electr. Eng.*, vol. 143, no. 3, pp. 231–241, May 1996.

[3] L. Morel, H. Godfroid, A. Miraian, and J. M. Kauffmann, "Doubly-fed induction machine: Converter optimization and field oriented control without position sensor," *Proc. Inst. Electr. Eng.*, vol. 145, no. 4, pp. 360–368, Jul. 1998.
[4] R. Datta and V. T. Ranganathan, "A simple position-sensorless algorithm for rotor-side field-oriental control of wound-rotor induction machine," *IEEE Trans. Ind. Electron.*, vol. 48, no. 4, pp. 786–793, Aug. 2001.
[5] R. Cardenas, R. Pena, J. Proboste, G. Asher, and J. Clare, "MRAS observer for sensorless control of standalone doubly fed induction generators," *IEEE Trans. Energy Convers.*, vol. 20, no. 4, pp. 710–718, Dec. 2005.
[6] B. Shen, V. Low, and B. T. Ooi, "Slip frequency phase lock loop (PLL) for decoupled P-Q control of doubly-fed induction generator (DFIG)," presented at the 2004 IEEE Ind. Electron. Soc. Conf., Busan, South Korea, Nov.
[7] B. Shen and B. T. Ooi, "Novel sensorless decoupled P-Q control of doubly-fed induction generator (DFIG) based on phase locking to γ–δ frame," presented at the 2005 Power Electron. Spec. Conf., Recife, Brazil, Jun.
[8] B. Shen and B. T. Ooi, "Parameter-insensitive sensorless decoupled P-Q controller for doubly-fed induction generator," in *Proc. 2007 IEEE Power Electron. Spec. Conf.*, Jun., pp. 2102–2107.
[9] B. T. Ooi, B. Shen, and V. Low, "System and method of controlling a doubly-fed induction generator," provisional U.S. Patent 60 867 510, Nov. 28, 2006.

Bakari Mwinyiwiwa (S'88–M'89) received the B.Sc. (Eng.) degree from the University of Dar es Salaam, Dar es Salaam, Tanzania, in 1985, and the M.Eng. and Ph.D. degrees from McGill University, Montreal, QC, Canada, in 1989 and 1997, respectively.

He is currently with the Department of Electrical Power Engineering, University of Dar es Salaam. His current research interests include high-power electronics and applications.

Yongzheng Zhang (S'06) received the M.A.Sc. degree in electrical engineering from Concordia University, Montreal, QC, Canada, in 2007. He is currently working toward the Ph.D. degree at the Department of Electrical and Computer Engineering, McGill University, Montreal.

His current research interests include renewable energy, application of converter for distributed generation, and electric machinery.

Baike Shen (M'07) was born in GuangXi, China. He received the B.Eng. degree in electrical engineering from Tsinghua University, Beijing, China, and the M.Eng. degree from McGill University, Montreal, QC, Canada.

He was with GuangXi Power Company. He is currently with the British Columbia Transmission Corporation (BCTC), Vancouver, BC, Canada. His current research interests include power electronics and power systems.

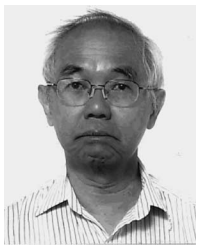

Boon-Teck Ooi (S'69–M'71–SM'85–F'03–LF'05) was born in Malaysia. He received the B.Eng. (Hons.) degree from the University of Adelaide, Adelaide, S.A., Australia, the S.M. degree from Massachusetts Institute of Technology, Cambridge, and the Ph.D. degree from McGill University, Montreal, QC, Canada.

He is currently a Professor in the Department of Electrical and Computer Engineering, McGill University.